Published on 09 September 2014. Downloaded by Pohang University of Science and Technology on 09/05/2015 08:15:26.

PCCP

ROYAL SOCIETY OF CHEMISTRY

PAPER

View Article Online
View Journal | View Issue

Cite this: *Phys. Chem. Chem. Phys.*, 2014, **16**, 22687

Single-crystalline CdTe nanowire field effect transistors as nanowire-based photodetector†

Mehrdad Shaygan,[a] Keivan Davami,[a] Nazli Kheirabi,[a] Changi Ki Baek,[b] Gianaurelio Cuniberti,[c] M. Meyyappan[d] and Jeong-Soo Lee*[a]

Received 26th July 2014, Accepted 9th September 2014

DOI: 10.1039/c4cp03322a

www.rsc.org/pccp

The electronic and photoconductive characteristics of CdTe nanowire-based field effect transistors were studied systematically. The electrical characterization of a single CdTe nanowire FET verifies *p*-type behavior. The CdTe NW FETs respond to visible-near infrared (400–800 nm) incident light with a fast, reversible and stable response characterized by a high responsivity (81 A W^{-1}), photoconductive gain ($\sim 2.5 \times 10^4$%) and reasonable response and decay times (0.7 s and 1 s, respectively). These results substantiate the potential of CdTe nanowire-based photodetectors in optoelectronic applications.

1. Introduction

Interesting properties of inorganic nanowires (NWs), together with controllable synthesis techniques, make them promising candidates for applications in nanoscale electronics, thermoelectric devices, optoelectronics, biosensors and other areas.[1] Among various types of optoelectronic devices, photodetectors, which convert optical input signals into electrical output signals, have witnessed a great deal of interest in medical imaging techniques, optical communication, intrachip optical interconnects and optoelectronic circuits.[2,3] The unique properties of nanowires such as high sensitivity, high wavelength selectivity, fast response, light polarization sensitivity, light absorption enhancement and high photoconductive gain are ideal for photodetectors in the above mentioned applications. The high sensitivity of nanowire-based detectors is owed to the large surface-to-volume ratio and reduced dimension of the detecting area. Deep surface trap states as a result of large surface-to-volume area could prolong the photocarrier lifetime and a short transit time could be obtained by reduced active area.[4]

CdTe with a direct band gap of 1.44 eV and a high absorption coefficient at room temperature has received attention for its potential in solar energy conversion devices, sensors and photonics,[5,6] high-efficiency photovoltaic devices[7,8] and light emitting diodes.[9,10] In contrast to the widely investigated photovoltaic application of CdTe, there have been only a few reports on photodetection, especially using nanowires.[4] The main challenge facing the photodetector application of CdTe NWs involves availability of efficient synthesis techniques to grow nanowires with high purity, good crystallinity and uniform morphology together with a suitable control of their diameter and length. CdTe nanowires have been grown by various methods including the solution–liquid–solid (SLS) method,[11,12] template-directed electrodeposition,[13] chemical vapor deposition[14] and the solvothermal method.[15] Each of these routes has some drawbacks, for example, the collapsing and aggregating of the nanowires after template removal.[11] In this regard, catalyzed vapor–liquid–solid (VLS) growth has emerged as a desirable technique for growing a variety of inorganic nanowires.[1,4] Here, we have synthesized single-crystalline CdTe nanowires *via* the VLS route and fabricated field effect transistors (FETs). Evaluation of the photoresponse characteristics of the FETs revealed that CdTe NW-based photodetectors show high responsivity, high photoconductive gain and significant stability in response to a wide range of irradiating light spectra.

2. Experimental procedure

The CdTe nanowires were synthesized *via* a vapor–liquid–solid (VLS) technique on silicon substrates covered with a 1 nm gold layer, as described in detail in the ESI.† The morphology of the samples was characterized using a field emission scanning electron microscope (SEM) (Philips XL 30S) operating at 5 kV, and an energy-dispersive X-ray spectroscope (EDS) was used to obtain their elemental composition. Following ultrasonic dispersion of the nanowires in ethanol, drops of the solution were deposited on a holly copper grid with a carbon film for examination by a high resolution transmission electron

[a] *Department of IT Convergence Engineering, Pohang University of Science and Technology (POSTECH), Pohang, South Korea. E-mail: ljs6951@postech.ac.kr*
[b] *Department of Creative IT Engineering (CITE), Pohang University of Science and Technology (POSTECH), Pohang, South Korea*
[c] *Institute for Materials Science and Max Bergmann Center of Biomaterials, TU Dresden, Dresden 01062, Germany*
[d] *NASA Ames Research Center, Moffett Field, CA 94035, USA*

† Electronic supplementary information (ESI) available: Experimental details and additional data. See DOI: 10.1039/c4cp03322a

microscope, (JEOL-2100F with Cs Corrected STEM) operating at 200 kV.

The structural characterization of the samples was carried out using a X-ray diffractometer (D/Max-2500/PC from Rigaku Co.), using Cu-Kα (λ = 1.5418 Å) radiation at 100 mA, 40 keV. The XRD patterns were recorded in the range of scanning angle 5°–90° at a scanning speed of 4° min^{-1}. The joint committees of powder diffraction standards (JCPDS) card file data were used to interpret the pattern and identify the observed peaks. The standard diffraction patterns of CdTe (JCPDS card no. 15-0770) and SiO_2 (JCPDS card no. 79-1912) were assigned as references. Raman spectroscopy was performed using a Senterra Raman spectroscope (Bruker Optics) using an excitation wavelength of 532 nm from a YAG laser. The spot size of the laser was 500 nm in diameter and an optical microscope was used to choose the probing area. The laser power for all the samples was 10 mW, selected to prevent damaging of the nanowires due to local heating effects. The as-grown samples on silicon substrates were used for Raman analysis without any special sample preparation.

To fabricate CdTe FETs, the nanowires were removed from the substrate by sonicating in ethanol solution followed by dispersing onto another Si substrate (a *p*-type substrate with a 300 nm oxide layer). The metal electrode pads were defined by a photolithographic masking technique with an area of 80 μm^2 and a 3–5 μm distance between neighboring pads. The electrodes were formed by depositing chromium/gold (30 nm/180 nm) layers *via* thermal evaporation, and ultimately a lift off process. Finally, CdTe NW FETs were fabricated with two metal contacts as source and drain electrodes and the Si substrate serving as a back gate. The electrical characteristics of the devices were measured using an Agilent 4156C semiconductor parameter analyzer with a probe station. The photoresponse characteristics of the CdTe NW-based photodetector were measured using a light source of a 500 W-tunable Hg(Xe) lamp and a monochromator (Cornerstone 130) to generate monochromatic light form 300 to 900 nm.

3. Results and discussion

Fig. 1 shows SEM images of CdTe nanowires grown by the VLS technique, yielding a mat of high density nanowires 35–150 nm in diameter and several microns long (panel a). An enlarged view in Fig. 1b reveals the diameter to be 45.2 nm and the gold particle at the tip of the NW confirms the VLS mechanism. The HRTEM image of the CdTe nanowire in Fig. 1c shows a lattice spacing of ~0.36 nm corresponding to the (111) plane of CdTe in zincblend structure. The well-defined diffraction spots in selected area diffraction pattern (SAED) confirm the single crystalline nature of the grown material. The EDAX spectrum of the nanowire stem (not shown here) indicated the presence of only Cd and Te in a near stoichiometric ratio (Cd/Te = 51.34 : 48.66 wt%), whereas EDAX recorded near the tip of the nanowire revealed the presence of Au, Cd, and Te, confirming the Cd–Te–Au alloy nature of the droplet (Fig. 1d). A detailed parametric study of the growth characteristics, optimized conditions and further characterization of the nanowires through

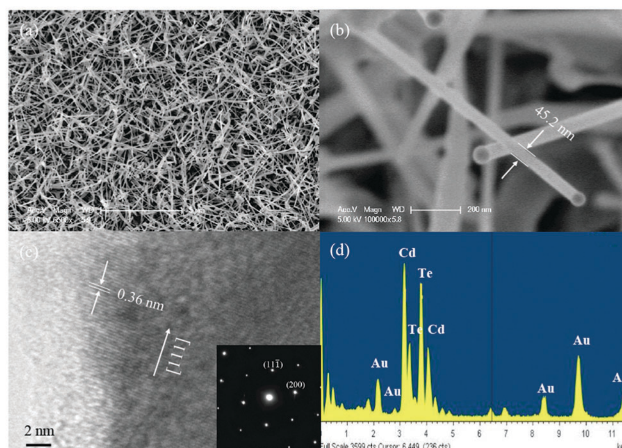

Fig. 1 (a) SEM image of a mat of CdTe nanowires grown by VLS. (b) High-magnification SEM image of an individual CdTe nanowire. (c) HRTEM image of a single crystalline CdTe nanowire; SAED pattern in the inset. (d) EDAX analysis of CdTe nanowires taken near the tip of nanowires.

X-ray diffraction and Raman spectroscopy are provided in the ESI.†

A top-view SEM image of a single CdTe NW field effect transistor with the Au electrode pads is shown in Fig. 2. The channel length (L) of this FET is 4.4 μm and the diameter of the nanowire is 49 nm. The drain current (I_{ds}) *versus* drain-source voltage (V_{ds}) was measured at gate voltages (V_g) varying from −12.5 V to 12.5 V to assess the electrical characteristics (Fig. 2c). The current is of the order of picoAmperes and the *I–V* curves demonstrate a nonlinear behavior due to the Schottky barrier formed on the metal semiconductor interfaces.[16–18] Fig. 2d presents the drain current *versus* gate voltage obtained at a constant V_{ds} = 5 V where the conductance of the nanowire increases as the gate voltage increases in negative polarity. From the linear region of the curve, the threshold gate voltage (V_{th}) and the transconductance ($g_m = dI_{ds}/dV_g$) can be extrapolated as −11 V and 32.3 pS, respectively.

The carrier mobility (μ_h) in a typical cylindrical nanowire with radius r can be expressed as:[19,20]

$$\mu = \frac{dI}{dV_g} \times \frac{\ln(2h/r)}{2\pi\varepsilon_o\varepsilon_r} \times \frac{L}{V_{ds}} \quad (1)$$

$$C = \frac{2\pi\varepsilon_o\varepsilon_r L}{\ln(2h/r)} \quad (2)$$

$$p = \frac{CV_{th}}{e\pi r^2 L} \quad (3)$$

where V_g is the gate voltage, e is the electronic charge, ε_o is the dielectric constant of vacuum, ε_r is the relative dielectric constant of gate insulator material (3.9 for SiO_2), h is the thickness of gate insulator film, L is the channel length and C is the nanowire capacitance. The estimated values of C and μ_h are 6.77×10^{-1} pF and 0.0042 $cm^2\ V^{-1}\ s^{-1}$, respectively; the mobility is close to the reported value for CdTe nanoribbons (NRs) but relatively low compared to bulk CdTe crystals and

Published on 09 September 2014. Downloaded by Pohang University of Science and Technology on 09/05/2015 08:15:26.

Published on 09 September 2014. Downloaded by Pohang University of Science and Technology on 09/05/2015 08:15:26.

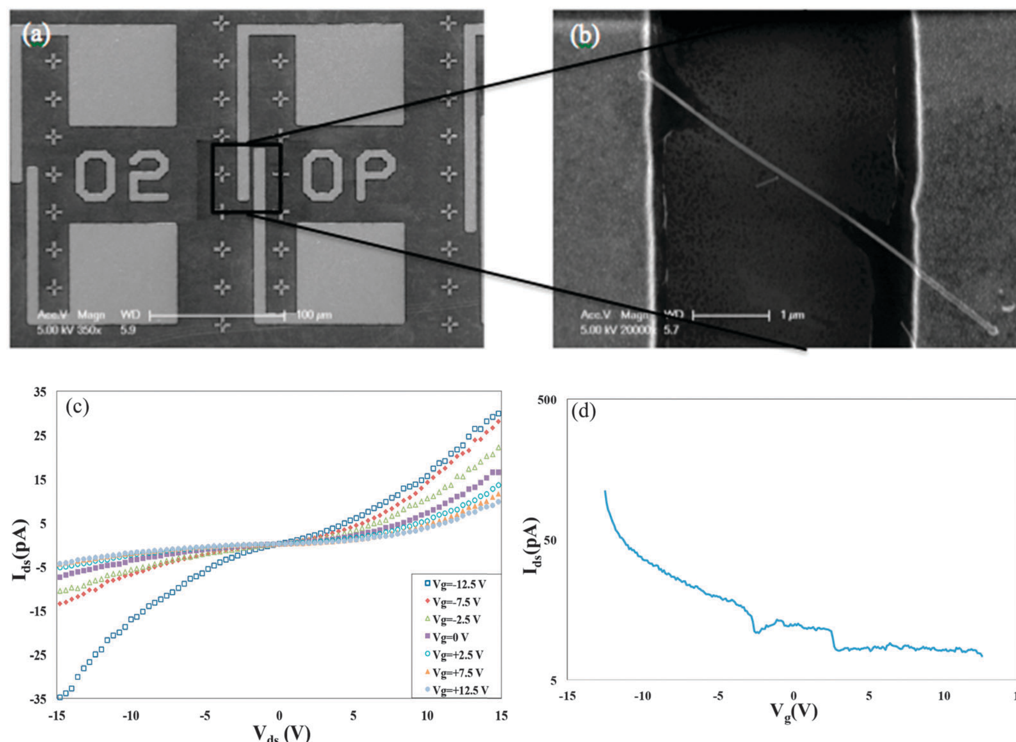

Fig. 2 (a) SEM image of a single CdTe NW field effect transistor. (b) Magnification of the device shown in (a). (c) I_{ds}–V_{ds} measured at gate voltages (V_g) varying from −12.5 V to 12.5 V, (d) drain current (log scale) *versus* gate voltage curves obtained at a constant V_{ds} = 5 V.

thin films.[18,21] The carrier mobility is affected by the inherent characteristics of the nanostructure such as crystallinity, the doping level and surface scattering[22] and the nature of the device itself such as top-gate/back-gate, channel length and type of dielectric material.[23] The observed low carrier mobility here can be attributed to the surface scattering of the CdTe nanowires, the low dielectric constant of the SiO_2 layer and the back gate structure of our FET devices which all could weaken the gating effect and the FET carrier mobility.[18,24] The hole concentration (p) is estimated to be 2.5×10^{18} cm^{-3} which is higher than that for CdTe nanoribbons but an order of magnitude lower than that of CdTe NWs measured by Li *et al.*[24]

To study the performance of a CdTe nanowire device as a photodetector, the device was illuminated with vertical monochromatic light and the corresponding I–V curves were recorded (Fig. 3a). Fig. 3b shows typical current *versus* voltage relation under dark and illuminated conditions with the light intensity kept constant at 550 μW cm^{-2}. The nonlinear behavior of the I–V curves is indicative of the Schottky contacts between the NW and Cr/Au electrodes. The CdTe NW photodetector is sensitive to visible and near infrared (NIR) while the photocurrent at an identical voltage decreases with the wavelength. The enhanced absorption of high-energy photons at or near the surface region of the semiconductor material could be the main reason for the commonly observed drop in sensitivity.[25] The generation of electron–hole pairs by photons with a higher energy than the bandgap originates the photocurrent. The conductivity of the photodetector can be modulated by these photogenerated carriers revealing the important role of the bandgap of the material in the determination of the dynamic range of photodetectors.[2] The bias voltage (V_{ds}) for all the measurements was set at 10 V. The I–V curves of the CdTe NW photodetector under illumination with 400 nm light of various intensities are shown in Fig. 3c. Clearly, the photocurrent at an identical voltage increases with the enhancement of light intensity. Under the light intensity of 78 μW cm^{-2}, the photoconductance reaches about 0.134 pS while by increasing the light intensity to 550 μW cm^{-2}, the photoconductance raises to 2.54 pS, resulting in a photosensitivity of about 19. This rate of photosensitivity is higher than that for CdTe nanorods and nanoribbons as shown in Table 1.

The dependence of photocurrent on light intensity is often described by the following equation as a power law:

$$I = AP^{\theta} \quad (4)$$

where I is the photocurrent, A is a constant for a selected wavelength, P is the light intensity and θ is an empirical value.[26] Generally, θ values less than unity have been observed in different nanostructure-based photodetectors such as ZnO nanowires,[26] CdS nanoribbons,[25] and $In_2Ge_2O_7$ nanobelts[27] due to a complex electron–hole generation and a recombination process within the semiconductor material.[28] Here, the data fitted to eqn (4) give 0.3 for θ which is higher than the reported values of other nanostructures of CdTe. As seen in Fig. 3d, the photocurrent increases gradually with the illumination intensity which could be due to the saturation of photoresponse at higher intensities as a result of the reduced number of available hole-traps at the surface of the semiconductor.[3] The photocurrent has

Published on 09 September 2014. Downloaded by Pohang University of Science and Technology on 09/05/2015 08:15:26.

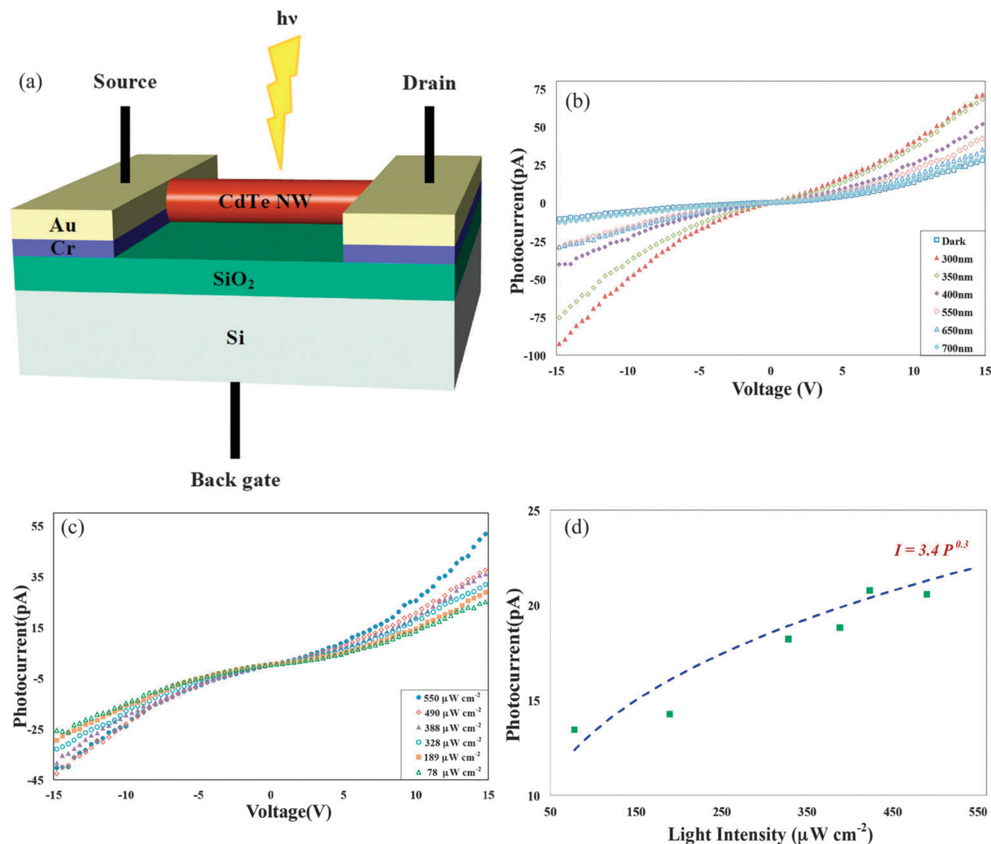

Fig. 3 (a) Schematic view of the fabricated CdTe NWFET photodetector under light illumination. (b) I–V relation of a CdTe nanowire photodetector in dark and under illumination with various wavelengths of light. (c) I–V curves of CdTe NW photodetector under illumination with 400 nm light of various intensities. (d) Dependence of photocurrent of CdTe NW on light intensity and the fitted curve according to the power law.

Table 1 A comparison of the CdTe NW photodetectors from this work with reports from the literature

Photodetector	R_λ (A W^{-1})	G (%)	Response, decay time	Photosensitivity	Dimension	Ref.
ZnSe nanobelt	0.12	37.2	<0.3 s, <0.3 s	na	5 μm (l) × 250 nm (w)	30
ZnSe nanowire	22	6810	na	na	80 nm (dia.) × 4 μm (l)	29
CdS nanobelt	na	na	1 s, 3 s	1.5 × 10^3	200 nm (w)	36
CdS nanowire	na	na	~15 ms, ~15 ms	39	200 nm (dia.) array	38
CdSe nanowire	na	5	20 μs, 30 μs	10–100	200 nm (w) × 60 nm (h) array	31
CdTe nanoribbon	7.8 × 10^2	2.4 × 10^5	1.1 s, 3.3 s	2	na	18
CdTe kinked NW	19.2	na	na	na	150 nm (dia.) × 2 (l) μm	34
CdTe nanorod	na	na	na	11	na	39
This work	80.1	2.5 × 10^4	0.7 s, 1 s	19	49.1 nm (dia.) × 4.39 (l) μm	

a sub-linear dependence on light intensity. At higher intensities, the number of available hole-traps is significantly decreased leading to the saturated photoresponse. In such a case, the density of free carriers can be obtained by

$$N = \frac{\eta F}{AL} T_1(F) \tag{5}$$

$$T_1(F) = T_1^0 \frac{1}{1 + (F/F_0)^n} \tag{6}$$

where η is the carrier photogeneration quantum efficiency, F is the photon absorption rate, A and L are the nanowire cross section and length, and T_1 is the carrier life time. By filling the traps, the number of free holes raises which increases the probability of electron–hole recombination. In the above equation, $T_1(F)$ is a carrier life time which is dependent on the absorption rate, T_1^0 is the carrier lifetime at low excitation density, F_0 is the photon absorption rate after saturation of traps and n is a fitting factor. The photocurrent (I_{ph}) can be expressed as

$$I_{ph} = qN\nu A = q\eta\left(\frac{T_1^0}{T_1}\right)\frac{1}{1 + (F/F_0)^n} \tag{7}$$

where the carrier drift velocity is $\nu = \eta V/l$ and q is the elementary charge.[3]

The key parameters determining the performance of photodetectors are responsivity (R_λ) and external quantum efficiency (EQE) or photoconductive gain (G) besides response time and detectivity. A high photoconductive gain is important to have a

 This journal is © the Owner Societies 2014

Published on 09 September 2014. Downloaded by Pohang University of Science and Technology on 09/05/2015 08:15:26.

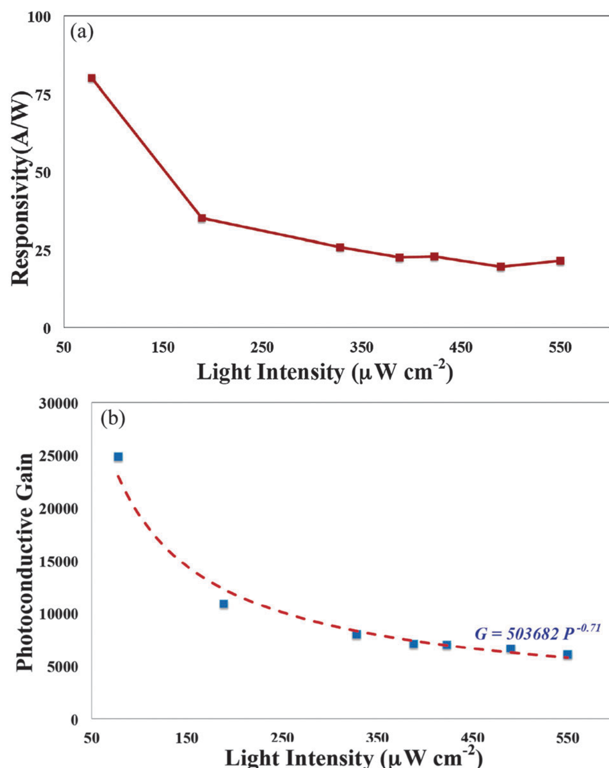

Fig. 4 (a) Dependence of responsivity and photoconductive gain on light intensity for a wavelength of 400 nm shown in (a) and (b), respectively.

high detectivity, while the dark current and noise have to be low as well. Photoconductive gain is defined as the number of charge carriers passing between the electrodes for each photon absorbed per second and the responsivity of a photodetector (R_λ) is defined as the generated photocurrent per unit of light power incident on the effective area of the detector. The R_λ and G can be expressed as follows:[4,18]

$$R_\lambda = I_{ph}/(P_{opt}S) \quad (8)$$

$$G = (I_{ph}/q)/(P_{opt}S/h\nu) = \tau/t_{tran}$$

where I_{ph} is the photocurrent, P is the incident light intensity, S is the effective illuminated area, q is the electronic charge, h is Planck's constant, ν is the frequency of incident light, τ is the carrier life time and t_{tran} is the carrier transit time.

Fig. 4 shows the dependence of responsivity and photoconductive gain on light intensity for a wavelength of 400 nm. At 78 μW cm^{-2}, the responsivity and photoconductive gain of the CdTe NW are 80.1 A W^{-1} and 2.5 × 10^4%, respectively, while for the intensity of 550 μW cm^{-2} the corresponding values decrease to 21.4 A W^{-1} and 6 × 10^3%, respectively. As shown in Table 1, these values are higher than those reported for photodetectors based on ZnSe nanowires (22 A W^{-1}),[29] ZnSe nanobelts (R_λ ~ 0.12 A W^{-1} and G ~ 37%),[30] CdSe nanowires (5%)[31] but lower than those of ZnO nanowires (G ~ 2 × 10^8)[3] and CdS nanobelts (R_λ ~7 × 10^4 A W^{-1}, G ~ 1.9 × 10^7%).[32] Interestingly, the performance here is higher than that of other CdTe nanostructures such as quantum dots (R_λ ~ 0.18 A W^{-1})[33] and high-crystalline kinked nanowires (R_λ ~ 19.2 A W^{-1})[34] but lower than for nanoribbons (R_λ ~ 7.8 × 10^2 A W^{-1}, G ~ 2.4 × 10^5%).[18] The significant high responsivity and gain of CdTe NR photodetectors are attributed to high-density traps induced by the surface modification of NRs through adsorption of water and oxygen molecules on the NR surface.[18] Both G and R_λ decrease with an increase in light intensity which could be due to: (i) the carrier-trap saturation at high light intensity which increases the electron–hole recombination by reducing the carrier lifetime;[3] (ii) generally, there is an energy barrier for recombination of electron–hole pairs at the surface of the semiconductors due to the band bending phenomenon as a result of Fermi-level pinning. By increasing the intensity of incident light, the number of hole carriers in the center of the wire increases, which lowers the potential barrier confining the holes. This decreases the lifetime of the hole carriers and consequently reduces the G and R_λ of the photodetector.[18,35]

The time-dependent photoresponse was measured to study the rise and decay time upon switching the light on and off. Fig. 5a shows the photocurrent response of a CdTe NW photodetector upon 400 nm illumination measured for a ~50 s on/off cycle at different light intensities. The "on" and "off" state currents for all five cycles remain the same, which shows the reversibility and stability of the photodetector over the whole period of measurement. Fig. 5 also shows the enlarged portions in the 100–200 s and 250–350 s ranges corresponding to the on–off and off–on transitions, respectively. By data extraction and fitting with an exponential function, short rising and decay times, 0.7 and 1 s, respectively, are calculated; these metrics are faster than that reported for CdS nanobelts,[36] RuO_2/TiO_2 nanowires[37] but slower than for CdSe nanowires,[31] CdS nanowires[38] and ZnSe nanobelts.[30] More importantly, our CdTe NW photodetector shows a faster photoresponse compared to CdTe nanorods[39] and CdTe nanoribbons.[18] The long response and decay times of CdTe NWs (compared to the very fast response photodetector) are attributed to the fact that the trapping and untrapping rates are much slower than the rate of the carrier recombination process. After the light resource is cut off, the photocurrent still exists and the carriers do not sweep out of the device for some time. These carriers, which are immobile holes and yet to recombine, make the photocurrent remain after the light source is off.[40] There is a trade-off between the response time and gain. Importantly, the existence of traps could prolong the carrier lifetime by destroying the electron–hole recombination and deterioration of time response but on the other hand this could result in enhanced responsivity and photoconductive gain in photodetectors.[18] Table 1 summarizes the performance of the photodetectors fabricated here in relation to previous reports in the literature.

4. Conclusion

We have fabricated FETs using a single CdTe nanowire and evaluated their photoelectric performance. The electrical

Published on 09 September 2014. Downloaded by Pohang University of Science and Technology on 09/05/2015 08:15:26.

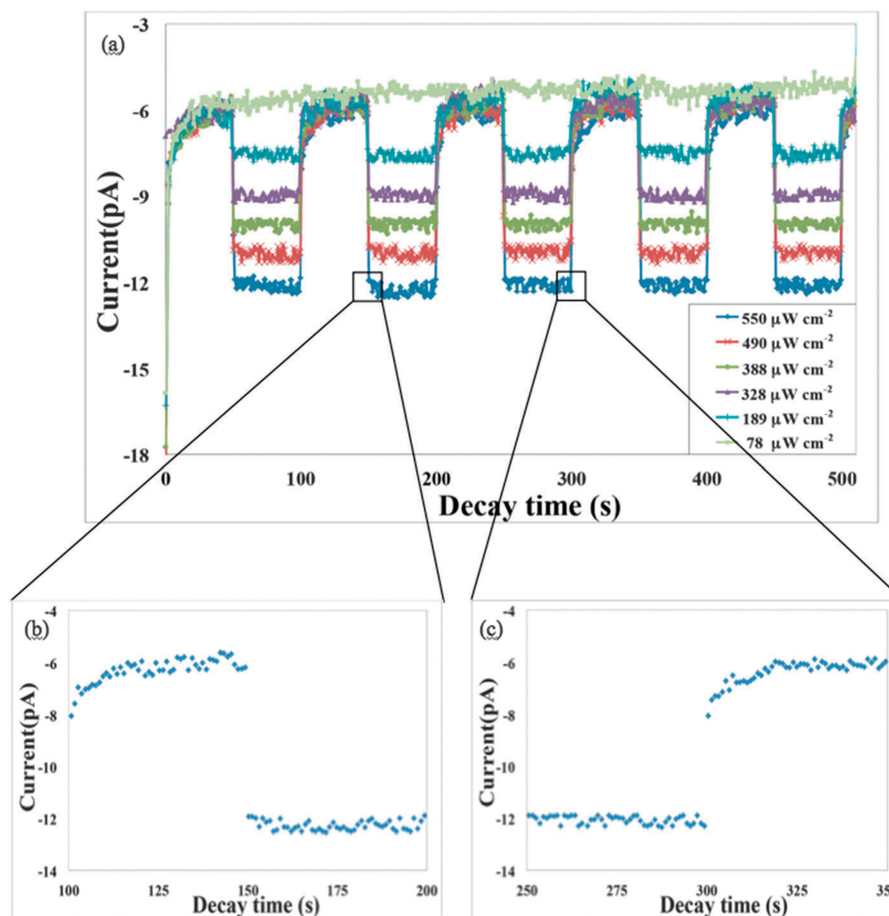

Fig. 5 (a) Photocurrent response of a CdTe NW photodetector upon 400 nm illumination measured for the light-on and light-off conditions with a ~50 s cycle at different light intensities. Enlarged portions of the (b) 100–200 s range (light-on to light-off) and (c) the 250–350 s range (light-off to light-on), both showing fast responses.

characterization of a single CdTe nanowire FET verifies *p*-type behavior. The CdTe NW FETs respond to visible-NIR (400–800 nm) incident light with a fast, reversible and stable response depicting a high responsivity (80.1 A W^{-1}), photoconductive gain ($\sim 2.5 \times 10^4$%) and reasonable response (0.7 s and 1 s for both response and decay time, respectively). The photoresponse performance of the CdTe based FETs here is superior to other telluride, sulfide and selenide based detectors reported in the literature. Though photodetectors based on one dimensional structures have continually improved, many challenges remain.[4] Precise control of nanowire diameter and quality including defects, traps and surface states is critical to developing reliable devices. Technologies to achieve controlled contact properties and large wafer fabrication are also needed to commercialize nanowire based optoelectronic devices.

Acknowledgements

This work was supported by the World Class University program through the National Research Foundation of Korea funded by the Ministry of Education, Science and Technology under Project R31-2008-000-10 100-0.

References

1 M. Meyyappan and M. Sunkara, *Inorganic nanowires: applications, properties and Characterization*, CRC Press, Boca Raton, FL, 2010.
2 T. Zhai, X. Fang, M. Liao, X. Xu, L. Li, B. Liu, Y. Koide, Y. Ma, J. Yao, Y. Bando and D. Golberg, *ACS Nano*, 2010, **4**, 1596–1602.
3 C. Soci, A. Zhang, B. Xiang, S. A. Dayeh, D. P. R. Aplin, J. Park, X. Y. Bao, Y. H. Lo and D. Wang, *Nano Lett.*, 2007, **7**, 1003–1009.
4 M. Shaygan, M. Meyyappan and J. S. Lee, Nanowire Field Effect Transistors in Optoelectronics, in *Nanowire Field Effect Transistors: Principles and Applications*, ed. D. M. Kim and Y. H. Jeong, Springer, 2014, pp. 187–224.
5 Z. Tang, N. A. K. Kotov and M. Giersig, *Science*, 2002, **297**, 237–240.
6 A. R. Flores, R. Castro-Rodriguez, J. L. Pena, N. Romeo and A. Bosio, *Appl. Surf. Sci.*, 2009, **255**, 7012–7016.
7 Y. Li, R. Mastria, A. Fiore, C. Nobile, L. Yin, M. Biasiucci, G. Cheng, A. M. Cucolo, R. Cingolani, L. Manna and G. Gigli, *Adv. Mater.*, 2009, **21**, 4461–4466.
8 B. L. Williams, D. P. Halliday, B. G. Mendis and K. Durose, *Nanotechnology*, 2013, **24**, 135703.

Published on 09 September 2014. Downloaded by Pohang University of Science and Technology on 09/05/2015 08:15:26.

9 H. Shen, Y. Zheng, H. Wang, W. Xu, L. Qian, Y. Yang, A. Titov, J. Hyvonen and L. S. Li, *Nanotechnology*, 2013, **24**, 475603.
10 Y.-W. Lin, W.-L. Tseng and H.-T. Chang, *Adv. Mater.*, 2006, **18**, 1381–1386.
11 Y. M. Sung, W. C. Kwak and T. G. Kim, *CrystEngComm*, 2012, **14**, 389–392.
12 F. Jiang, J. Liu, L. Fan, Y. Ding and Y. li, *Adv. Funct. Mater.*, 2012, **22**, 2402–2411.
13 H.-W. Liang, S. Liu and S.-H. Yu, *Adv. Mater.*, 2010, **22**, 3925–3937.
14 M. I. B. Utama, Z. Peng, R. Chen, B. Peng, X. Xu, Y. Dong, L. M. Wong, S. Wang, H. Sun and Q. Xiong, *Nano Lett.*, 2011, **11**, 3051–3057.
15 Q. Yang, K. Tang, C. Wang, Y. Qian and S. Zhang, *J. Phys. Chem. B*, 2002, **106**, 9227–9230.
16 G. S. Khripunov, *Semiconductors*, 2006, **40**, 113–117.
17 M. C. Kum, B. Y. Yoo, Y. W. Rheem, K. N. Bozhilov, W. Chen, A. Mulchandani and N. V. Myung, *Nanotechnology*, 2008, **19**, 325711.
18 X. Xie, S.-Y. Kwok, Z. Lu, Y. Cao, L. Luo, J. A. Zapien, I. Bello, C.-S. Lee and W. Zang, *Nanoscale*, 2012, **4**, 2914–2919.
19 E. N. Dattoli, Q. Wan, W. Guo, Y. Chen, X. Pan and W. Lu, *Nano Lett.*, 2007, **7**, 2463–2469.
20 O. Wunnicke, *J. Appl. Phys.*, 2006, **89**, 083102.
21 M. Takahashi, K. Uoasaki, H. Kita and S. Yamaguchi, *J. Appl. Phys.*, 1986, **60**, 2046–2049.
22 J. Jie, W. Zhang, I. Belo, C.-S. Lee and S.-T. Lee, *Nano Today*, 2010, **5**, 313–336.
23 Z. He, W. Zhang, W. Zhang, J. Jie, L. Luo, G. Yuan, J. Wang, C. M. L. Wu, I. Bello, C. S. Lee and S. T. Lee, *J. Phys. Chem. C*, 2010, **114**, 4663–4668.
24 S. Li, X. Li and H. Zhao, *Micro Nano Lett.*, 2013, **8**, 308–310.
25 J. S. Jie, W. J. Zhang, Y. Jiang, X. M. Meng, Y. Q. Li and S. T. Lee, *Nano Lett.*, 2006, **6**, 1887–1892.
26 H. Kind, H. Q. Yan, B. Messer, M. Law and P. D. Yang, *Adv. Mater.*, 2002, **14**, 158–160.
27 L. Li, P. S. Lee, C. Yan, T. Zhai, X. Fang, M. Liao, Y. Koide, Y. Bando and D. Golberg, *Adv. Mater.*, 2010, **22**, 5145–5149.
28 A. Rose, *Concepts in Photoconductivity and Allied Problems*, Krieger Publishing Company, New York, 1978.
29 J. Salfi, U. Philipose, C. F. de Sousa, S. Aouba and H. E. Ruda, *Appl. Phys. Lett.*, 2006, **89**, 261112.
30 X. Fang, S. Xiong, T. Zhai, Y. Bando, M. Liao, U. K. Gautam, Y. Koide, X. Zhang, Y. Qian and D. Golberg, *Adv. Mater.*, 2009, **21**, 5016–5021.
31 S.-C. Kung, W. E. van der Veer, F. Yang, K. C. Donavan and R. M. Penner, *Nano Lett.*, 2010, **10**, 1481–1485.
32 L. Li, P. Wu, X. S. Fang, T. Zhai, D. Li, M. Laio, Y. Koide, H. Q. Wang, Y. Bando and D. Golberg, *Adv. Mater.*, 2010, **22**, 3161–3165.
33 C.-C. Tu and L. Y. Lin, *Appl. Phys. Lett.*, 2008, **93**, 163107.
34 Y. Ye, L. Dai, T. Sun, L. P. You, R. Zhu, J. Y. Gao, R. M. Peng, D. P. Yu and G. G. Qin, *J. Appl. Phys.*, 2010, **108**, 044301.
35 A. Zhang, H. Kim, J. Cheng and Y. H. Lo, *Nano Lett.*, 2010, **10**, 2117–2120.
36 T. Gao, Q. H. Li and T. H. Wang, *Appl. Phys. Lett.*, 2005, **86**, 173105.
37 Y.-L. Chueh, C.-H. Hsieh, M.-T. Chang, L.-J. Chou, C. S. Lao, J. H. Song, J.-Y. Gan and Z. L. Wang, *Adv. Mater.*, 2007, **19**, 143–149.
38 Q. Li and R. M. Penner, *Nano Lett.*, 2005, **5**, 1720–1725.
39 X. Wang, J. Wang, M. Zhou, H. Zhu, H. Wang, X. Cui, X. Xiao and Q. Li, *J. Phys. Chem. C*, 2009, **113**, 16951–16953.
40 M. C. Kum, H. Jung, N. Chartprayoon, W. Chen, A. Mulchandani and N. V. Myung, *J. Phys. Chem. C*, 2012, **116**, 9202–9208.